Star formation across cosmic time with radio surveys. The promise of the SKA

Gianfranco De Zotti[1], Matteo Bonato[2,1] and Zhen-Yi Cai[3,4]

1. INAF-Osservatorio Astronomico di Padova, Vicolo dell'Osservatorio 5, I-35122 Padova, Italy
2. INAF, Osservatorio di Radioastronomia, Via Gobetti 101, I-40129, Bologna
3. CAS Key Laboratory for Research in Galaxies and Cosmology, Department of Astronomy, University of Science and Technology of China, Hefei, Anhui 230026, China
4. School of Astronomy and Space Science, University of Science and Technology of China, Hefei 230026, China

This lecture briefly reviews the major recent advances in radio astronomy made possible by ultra-deep surveys, reaching microJansky flux density levels. A giant step forward in many fields, including the study of the evolution of the cosmic star formation history is expected with the advent of the Square Kilometer Array (SKA).

1 Introduction

Ever since radio surveys reached sub-milliJansky[1] flux density levels, they have proved to be the primary means of identifying star-forming galaxies at high redshift. Observations have solidly demonstrated a tight correlation between the low-frequency radio continuum, dominated by synchrotron emission of relativistic electrons mostly produced by supernovae, and far-infrared (FIR) emission of galaxies.

Since the FIR is a well established measure of the star-formation rate (SFR) of galaxies, this correlation has legitimated the radio continuum emission as a tracer of SFR. However, so far radio surveys have only played a marginal role in the study of the cosmic star-formation history, mostly because of their sensitivity. But the radio astronomy is at the verge of a revolution, thanks to the square kilometre array (SKA), that will offer an observing window between 50 MHz and 24 GHz, extending to flux density limits more than three orders of magnitude deeper than it is currently possible, with unprecedented versatility.

This lecture briefly reviews the role of radio astronomical surveys towards our understanding of extragalactic sources. It focusses in particular on populations of faint (μJy) radio sources and discusses the advances expected from the future deeper surveys with the SKA and its precursors, and their impact on our understanding of the cosmic star-formation history.

The layout of the lecture is the following. Section 2 contains a general introduction to the radio sky. Section 3 presents general properties of classical radio sources, i.e. radio Active Galactic Nuclei (AGNs). Section 4 discusses the radio emission from star-forming galaxies. The identification of the faint (sub-mJy) population is dealt with in Section 5. Section 6 deals with radio quiet (RQ) AGNs, that were proposed as a new faint radio source population. Section 7 provides an introduction to the SKA and to its role in the study of the cosmic star-formation history. Finally, Section 8 summarizes the main conclusions.

[1] One Jansky (Jy) corresponds to $10^{-23}\,\mathrm{erg\,cm^{-2}\,s^{-1}\,Hz^{-1}} = 10^{-26}\,\mathrm{W\,m^{-2}\,Hz^{-1}}$.

2 Introduction to the radio sky

The radio sky is very different from what we are used to seeing in the optical. With few exceptions (the nearest galaxies like Andromeda or, in the southern hemisphere, the Magellanic Clouds, and Solar System objects) the brightest optical sources, visible with the naked eye, are stars. These are approximate blackbody radiators (thermal emitters). Their emission covers a relatively narrow range of frequencies, ranging from the ultraviolet (UV) to the infrared (IR), depending on the star temperature. As one goes fainter, at optical magnitudes $m \geq 19$–20 (in the AB system), galaxies take over. Most of their light is again of thermal origin, coming from stars, so is confined at UV to IR wavelengths.

But few stars are visible at radio frequencies. Most of the point sources visible on radio maps are distant (median redshift $z \sim 0.8$ for a broad range of detection limits; Condon, 1989) luminous radio galaxies (RGs) and quasars. The radio emission from RGs and quasars is non-thermal, and is due to ultra-relativistic ($E \gg m_{\rm e}c^2$) electrons moving in a magnetic field and thereby emitting synchrotron radiation, which, unlike blackbody emission, can cover a very large range in frequency, reaching up to ~ 10 decades in some sources.

The fact that bright radio sources are mostly at substantial redshifts has implied that, for several decades, extragalactic radio surveys remained the most powerful tool to probe the distant universe. Even "shallow" radio surveys, those of limited radio sensitivity, reach sources with redshifts predominantly above 0.5.

Since the 1960s, the most effective method for finding high-z galaxies has been the optical identification of radio sources, a situation persisting until the mid-1990s, when the arrival of the new generation of 8–10 m class optical/infrared telescopes, the refurbishment of the Hubble Space Telescope, the Lyman-break technique (Steidel et al., 1996) and the Sloan Digital Sky Survey (SDSS; York et al., 2000) produced an explosion of data on high-redshift galaxies.

Indeed radio surveys produced real revolutions in astrophysics and cosmology (de Zotti et al., 2010) :

- **Active Galactic Nuclei.** Radio emission provided the first evidence of non-stellar activity. Identifications of some of the sources detected by the earliest radio astronomical observations (Bolton et al., 1949; Ryle et al., 1950) showed that they are extragalactic (Ryle et al., 1950; Baade & Minkowski, 1954). The amount of energy in the radiating particles turned out to be huge, up to 10^{60} erg, for double-lobe radio galaxies (Burbidge, 1959), and difficult to account for.

- **Synchrotron emission.** Estimated brightness temperatures of radio sources could not be reconciled with thermal emission from interstellar gas. This led to the identification of synchrotron emission as the dominant continuum process producing the power-law spectra of radio sources (Alfvén & Herlofson, 1950; Shklovskii, 1952); see Ginzburg & Syrovatskii (1965) for an early review.

- Radio astronomy first **pushed the boundary of observable universe to cosmological distances**. Ryle & Scheuer (1955) argued that the isotropic distribution of "radio stars" placed the bulk of them beyond 50 Mpc. When arcminute positional accuracy became available (Smith, 1952) it was quickly

realized that the majority of the host galaxies were beyond the reach of the optical telescopes of the epoch. Minkowski (1960) measured a redshift of 0.46 for 3C295, the fifteenth brightest radio source at high Galactic latitude. This measurement remained the redshift record for a galaxy for 10 years. Efforts to identify and measure redshifts of bright radio sources led to the discovery that they are frequently located in rich clusters of galaxies. This was also the case for 3C295; measurement of its redshift led to the discovery of the most distant cluster known at the time. In 1965, the redshift record was 2.012 for the radio quasar 3C9 (Schmidt, 1965). Only after the turn of the century did the redshift record become routinely set by objects discovered in surveys other than at radio wavelengths (e.g., Stern, 2000).

- **The discovery of quasars**, starting with 3C273 (Hazard et al., 1963; Schmidt, 1963). Their extreme luminosities, 10 to 30 times higher than those of the brightest giant ellipticals, coming from very compact regions, called for *a new energy source*. Hoyle & Fowler (1963) were the first to argue that "only through the contraction of a mass of $10^7 - 10^8\,M_\odot$ to the relativistic limit can the energies of the strongest sources be obtained." Soon after, Salpeter (1964) showed that accretion into a "Schwarzschild singularity" can release an energy of $0.057\,c^2$ per unit mass, and thus can account for the quasar luminosity. A similar view was independently proposed by Zel'dovich (1964). The idea that the quasar luminosity comes from accretion onto a super-massive black hole gained momentum when Lynden-Bell (1969) argued that "collapsed bodies" (i.e. black holes) should be common in galactic nuclei. However, the alternative view of non-cosmological redshifts, was also held by some groups. For example Hoyle & Burbidge (1966) argued that quasars are coherent objects, ejected by galactic nuclei at relativistic speed. An argument in favour of a local origin of these objects was that relativistic electrons emitting optical and infrared synchrotron radiation would also boost up the energy of ambient photons by inverse Compton scattering. Repeated scatterings boost dramatically the inverse Compton luminosity, yielding a divergence called the "inverse Compton catastrophe". To avoid that Compton energy losses exceed the synchrotron losses, the magnetic field must be very strong, to the point that the lifetimes of electrons become extremely short, of order of seconds, making the cosmological interpretation of redshifts hardly tenable (Hoyle, 1966).
- **Relativistic beaming.** Woltjer (1966) pointed out that the Hoyle (1966) argument depends strongly on the assumed isotropy of relativistic electrons. If, as is dynamically more likely, electrons flow in a narrow cone (jet) along the field lines of a radial field, the difficulty is eliminated. *The discovery of superluminal motions* of quasar radio components (Cohen et al., 1971; Whitney et al., 1971) strongly supported the relativistic jet model. In fact Rees (1966) had predicted, five years before the discovery, that relativistic bulk motions at small angles with respect to the line-of-sight can produce apparent superluminal velocities. This led to the *development of unified models* of radio sources: quasars and radio galaxies are one and the same, with orientation of the axis to the viewer's line of sight determining classification via observational appearance (Antonucci & Miller, 1985; Barthel, 1989; Urry & Padovani, 1995).
- **History of the Universe**. Radio surveys highlighted a new global property

of the universe: *cosmological evolution*, disproving the then widely accepted Steady-State model. The debate generated by early radio surveys was passionate. The Steady-State versus Big Bang controversy was rooted in the simplest statistics to be derived from any survey: the integral source counts, the number of objects per unit sky area above given intensities or flux densities. As discussed by Ryle (1955) and Ryle & Scheuer (1955), the slope of such counts must be flatter than the Euclidean slope[2] of $-3/2$ in a Steady-State universe and in any reasonable Friedman model, if the source spatial distribution is independent of distance. But the source count from the 2C(ambridge) radio survey (Shakeshaft et al., 1955) showed an integral slope of approximately -3. Ryle (1955) and Ryle & Scheuer (1955) interpreted the 2C excess of faint sources in terms of the radio sources having far greater space density at earlier epochs and argued against the Steady-State theory. However, observations by Mills & Slee (1957) with the Sydney antenna did not confirm the steep 2C slope. These authors showed that confusion, i.e. the blending of weak, individually undetectable sources, to produce detectable signals, can have disastrous effects, and this affected the early Cambridge source counts. Still Mills et al. (1958), after correcting for source confusion and instrumental effects, found a slope of -1.65, steeper than the Euclidean slope although substantially flatter than the 2C slope. Scheuer (1957) developed the $P(D)$ technique, circumventing the confusion problem and showing that the interferometer results of 2C were consistent with the Sydney findings. Ryle & Clarke (1961) argued that observations of radio sources "appear to provide conclusive evidence against the steady-state model". But the damage had been done: some cosmologists, led by Hoyle, believed that radio astronomers did not know how to interpret their data.

- The **discovery of the Cosmic Microwave Background** (CMB) in 1965 constituted the definitive consecration of the Big Bang model (Penzias & Wilson, 1965; Dicke et al., 1965), thus making the 'source-count controversy' irrelevant in one sense. The initial slope of the low-frequency integral radio source counts was finally assessed at -1.8 (Ryle, 1968), confirming that Ryle's interpretation was right. While the discovery of CMB may indeed have shown that a Big Bang took place, the source counts demonstrated further that *objects in the Universe evolve either individually or as a population* – a concept not fully accepted by the astronomy community until both galaxy sizes and star-formation rates were shown to change with epoch.

- **Discovery of pulsars** (Hewish et al., 1968). In 1974 Hewish was awarded the Nobel prize in physics. Observations were done by his student Jocelyn Bell.

- **Discovery of the first pulsar in a binary system (Hulse & Taylor, 1975), allowing tests of general relativity in a strong gravitational field**. Such a compact system with rapidly orbiting masses would radiate large quantities of gravitational radiation. Taylor monitored the pulsar system for decades, finding that the shift of the periastron time is in close agreement

[2]In an Euclidean universe the number of sources N is proportional to the volume, i.e. to r^3 for a sphere; the flux density, S, is $\propto r^{-2}$ so that $N \propto S^{-3/2}$.

with predictions from general relativity. Russell Hulse and Joseph Taylor were awarded the Nobel Prize 1993.

- **Detection of primordial CMB anisotropies** (Smoot et al., 1992), shedding light on the origin of structure in the universe and opening the way to "precision cosmology".

For a more comprehensive list of the key discoveries from radio astronomy in the metre and centimetre wavebands see Wilkinson et al. (2004). The latter authors noted that "radio telescopes have set a large part of the current astronomical agenda", that "the largest radio telescopes of their day have dominated the discoveries" and that "most scientific advances follow technical innovation". Hence they conclude that the SKA, with its performances orders of magnitude better than those of present day radio instrumentation, brims with promises of transforming our view of the universe.

3 Generalities on radio AGNs

Source counts are currently recognized as essential data in delineating the different radio-source populations and in defining the cosmology of AGNs. These counts are dominated down to milli-Jansky (mJy) levels by the canonical radio sources, believed to be powered by super-massive black-holes (e.g., Begelman et al., 1984) in galactic nuclei.

By today's standards strong radio sources have flux densities $S \geq 1\,\mathrm{Jy}$, intermediate ones go down $\simeq 1\,\mathrm{mJy}$, and the deepest surveys reach μJy levels (for reviews, see de Zotti et al., 2010; Padovani, 2016; Padovani et al., 2017).

Radio-source spectra are usually described as power laws ($S_\nu \propto \nu^\alpha$)[3]. AGN-powered radio sources are traditionally classified in two main categories: steep- ($\alpha < -0.5$) and flat-spectrum ($\alpha > -0.5$). The early low-frequency (meter to decimeter wavelength) surveys, found radio sources almost exclusively of steep power-law form. Later surveys at cm-wavelengths found objects of diverse spectral types, and in general, anything which was not 'steep-spectrum' in form was called 'flat-spectrum'. However, truly flat-spectrum sources are rare.

From a physical point of view the flat-/steep-spectrum classification based on the low-frequency (typically $\simeq 1$ to $\simeq 5\,\mathrm{GHz}$) spectral index corresponds to the source compactness. Steep-spectrum sources are generally extended while the flat-spectrum ones are compact. In fact, in a compactness versus low frequency spectral index diagram there is a remarkably clean separation between steep-spectrum/extended sources and flat-spectrum/compact sources (cf. Fig. 4 of Massardi et al., 2011). There are however exceptions, such as the Compact Steep Spectrum (CSS) sources (e.g., Orienti, 2016).

Steep-spectra are optically thin synchrotron, while the "flat-spectra" are the superposition of multiple components, with different self-absorption frequencies. In general, however, each source has both a compact, flat-spectrum core and extended steep-spectrum lobes (cf., e.g., Fig. 2 of de Zotti et al., 2010). This already implies that a simple power-law representation can only apply to a limited frequency range. Self-absorption (synchrotron and free-free) can produce spectra rising with frequency at the low-frequency optically-thick regime, while at high frequencies the

[3]We note that this convention is not universal; some people still prefer the old 'Cambridge' convention $S_\nu \propto \nu^{-\alpha}$.

synchrotron emission becomes optically thin, power law, and energy losses of relativistic electrons ("electron ageing effect") translate into a spectral steepening.

According to the widely accepted "unification" scheme (Scheuer & Readhead, 1979; Orr & Browne, 1982; Scheuer, 1987; Barthel, 1989), the appearance of sources depends primarily on their axis orientation relative to the observer. This paradigm stems from the discovery of relativistic jets (Cohen et al., 1971; Moffet et al., 1972) giving rise to strongly anisotropic emission. A line of sight close to the source jet axis offers a view of the compact, Doppler-boosted, flat-spectrum base of the approaching jet. Doppler-boosted low-radio-power Fanaroff & Riley (1974), type I (FR I; edge-dimmed)] sources are associated with BL Lac objects, characterized by optically featureless continua, while the powerful type II (FR II; edge-brightened) sources are seen as flat-spectrum radio quasars (FSRQs). A third class of, mostly steep-spectrum, radio sources, FR 0, has been proposed by Baldi et al. (2015). These objects share many characteristics typical of FR I radio galaxies but have a more conspicuous radio core and extend a few kpc at most.

The view down the axis offers an unobstructed sight of the active nucleus which may outshine the starlight of the galaxy by five magnitudes. The source appears stellar, either as a FSRQ or as a BL Lac object. FSRQs and BL Lacs are collectively referred to as blazars. In the case of a side-on view, the observed low-frequency emission is dominated by the extended, optically thin, steep-spectrum components, the radio lobes; and the optical counterpart generally appears as an elliptical galaxy. A dusty torus (Antonucci & Miller, 1985) hides the active nucleus emission from our sight. At intermediate angles between the line of sight and the jet axis, angles at which we can see into the torus but the alignment is not good enough to see the Doppler-boosted jet bases, the object appears as a 'steep-spectrum quasar'.

4 Radio emission from star-forming galaxies

Counts down to mJy levels are accounted for by radio AGNs (cf. Fig. 3 of Massardi et al., 2010). As mentioned above, the shape of the counts demonstrates that these objects undergo a strong cosmological evolution. But when radio surveys reached sub-mJy flux density levels (Windhorst et al., 1984; Condon & Mitchell, 1984), the Euclidean normalized counts showed a flattening or an upturn, indicating the emergence of a new population (for updated counts at 1.4 GHz see Padovani, 2016).

Windhorst et al. (1985), based on optical identifications available for less than half of the sample, suggested that "for $1 < S_{1.4} < 10$ mJy a blue radio galaxy population becomes increasingly important; these often have peculiar optical morphology indicative of interacting or merging galaxies". The identification by Kron et al. (1985) showed that "For $18.5 \leq V \leq 21.5$, about one-third of the mJy radio galaxies are bluer than the giant ellipticals. They are not morphologically like the brighter spirals, but rather are a different class of peculiar (interacting, merging, or compact) galaxies".

Only a few years earlier, in 1983, the InfraRed Astronomical Satellite (IRAS) had carried out an all sky survey at far-IR wavelengths, providing evidence of a galaxy population with star-formation rates much higher than normal spiral galaxies (starburst galaxies). Danese et al. (1987) showed that evolving starburst/interacting galaxies could easily account for the excess counts, for the observed colours and for the morphological properties. On the contrary, the data could not be interpreted in

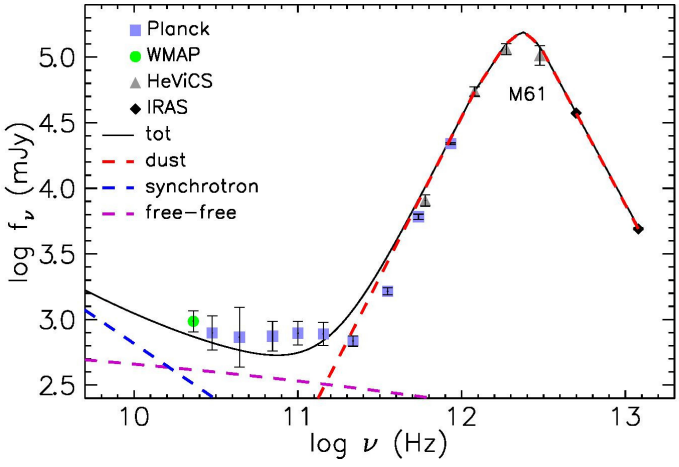

Fig. 1: Spectral energy distribution (SED) of the nearby star-forming galaxy M 61 showing the contributions of synchrotron (dashed blue line), free-free (dashed purple line) and dust (dashed red line) emissions. The solid black line shows the total. Sources of data points: *Planck* (open diamonds; Planck Collaboration et al., 2016); WMAP (filled circle Gold et al., 2011); the *Herschel* Virgo Cluster Survey (HeViCS, triangles; Pappalardo et al., 2015) and IRAS (diamonds). Note that photometric measurements of M 61 are complicated because it is quite extended (angular size of 6′, in the optical). On one side, the contributions of low surface density external regions are easily missed; on the other side, the low resolution *Planck* and *WMAP* measurements may also pick up contributions from our own Galaxy. Hence the true photometric errors may be substantially larger than the nominal ones shown in the figure. The lines are not fits to the data but are simply meant to illustrate the shape and the relative importance of the three contributions.

terms of a new population of unevolving low-luminosity radio sources or of normal spiral galaxies with evolution consistent with the observational constraints.

Although to really understand which sources were responsible for the flattening and sort out the source population of the sub-mJy radio sky took more than thirty years, it was already clear that the deep surveys were beginning to detect radio emission not of nuclear origin but associated to star-formation.

Determinations of the local radio luminosity function (Sadler et al., 2002; Mauch & Sadler, 2007) have shown that it has contributions from two populations. At 1.4 GHz the bright portion ($P_{1.4\mathrm{GHz}} \geq 10^{23}\,\mathrm{W\,Hz^{-1}}$) is dominated by canonical, steep-spectrum radio galaxies, whose luminosities reach $P_{1.4\mathrm{GHz}} \geq 10^{26}\,\mathrm{W\,Hz^{-1}}$. At lower luminosities star-forming galaxies (SFGs) take over. Luminosities of SFGs reach only $P_{1.4\mathrm{GHz}} \simeq 10^{24}\,\mathrm{W\,Hz^{-1}}$.

The radio emission of SFGs has two components, both related to star formation: synchrotron radiation from relativistic electrons and free-free emission from H II regions. The synchrotron emission results from relativistic plasma, thought to be accelerated primarily in supernova remnants (SNRs) associated with massive (mass larger than about $8\,M_\odot$) stars that end as Type II and Type Ib supernovae. Such massive stars live $\leq 3 \times 10^7$ yr, and the relativistic electrons probably have lifetimes $\leq 10^8$ yr (Condon, 1992). Thus the relativistic electrons emitting the synchrotron radiation

have propagated significant distances (≥ 1 kpc) from their short-lived ($\geq 10^5$ yr) and now defunct parent SNRs. Consequently the original sources of the relativistic electrons have disappeared, and their detailed spatial distribution has been smoothed beyond recognition (Condon, 1992). Moreover, the steps between star formation and synchrotron emission (supernova explosion, acceleration of relativistic electrons in the SNR, propagation of cosmic rays throughout the galaxy, energy loss, and escape) are poorly understood, impeding a quantitative interpretation of the observed synchrotron spectra and brightness distributions.

However there is a remarkably tight and ubiquitous correlation between the global FIR and the (predominantly synchrotron) radio luminosities of star forming galaxies (e.g., Yun et al., 2001). Except for galaxies with very low SFRs, the FIR luminosity appears to be a good measure of the bolometric luminosity produced by massive ($M \geq 5\,M_\odot$) young stars which are the most efficient dust heaters. Hence, also the synchrotron luminosity can be safely exploited as a measure of the SFR. Excluding objects with radio emission of nuclear origin, star forming galaxies lie very close to a linear relation between radio and FIR flux densities, with an rms scatter of less than 0.26 dex (Yun et al., 2001). The radio-FIR correlation was established for local galaxies, using IRAS data. However, more recent data, primarily from the *Herschel* observatory, have shown that it persists up to high redshifts (Ivison et al., 2010; Magnelli et al., 2015; Delhaize et al., 2017; Barger et al., 2012, 2017).

The massive stars ionize the H II regions as well, powering the free-free emission whose intensity is therefore proportional to the production rate of Lyman continuum photons. Thus, the free-free emission:

- allows the mapping of star-formation regions even in deeply dust-enshrouded regions;
- is a measure of the instantaneous star formation rate, while the information from the synchrotron is delayed by $\geq 10^7$ yr.

Radio maps can be made with sub-arcsec position accuracy and resolution, unambiguously identifying the most luminous star-forming regions within galaxies and resolving even the most compact ones. At radio wavelengths also the densest star-forming regions, generally associated to the most intense starbursts, are transparent, so that observed flux densities are accurately proportional to intrinsic luminosities. Radio stars are rare; therefore their contamination of emission from star-forming regions is generally negligible.

Synchrotron, with a spectral index $\alpha_{\rm sync} \sim -0.75$ ($S \propto \nu^\alpha$), generally dominates at rest-frame frequencies $\lesssim$ 22–30 GHz, and above $\sim$ 100–150 GHz the radio emission is overwhelmed by re-radiation of thermal dust, heated by young stars (cf. Fig. 1). Hence, the free-free emission, which has an effective spectral index at radio frequencies $\alpha_{\rm ff} \sim -0.1$, emerges only over a narrow frequency range: isolating it and measuring its flux density is observationally difficult. Note however the timescales. Most of the synchrotron radiation in a typical galaxy arises from fairly old ($\gtrsim 10^7$ yr) relativistic electrons. Hence, the radio emission in the youngest galaxies should be free-free. This is expected to be particularly relevant at the highest redshifts, when cosmic timescales are short.

A calibration of the *SFR-synchrotron emission* relation was obtained by Murphy et al. (2011) using Starburst99 (Leitherer et al., 1999) for a specific choice of the

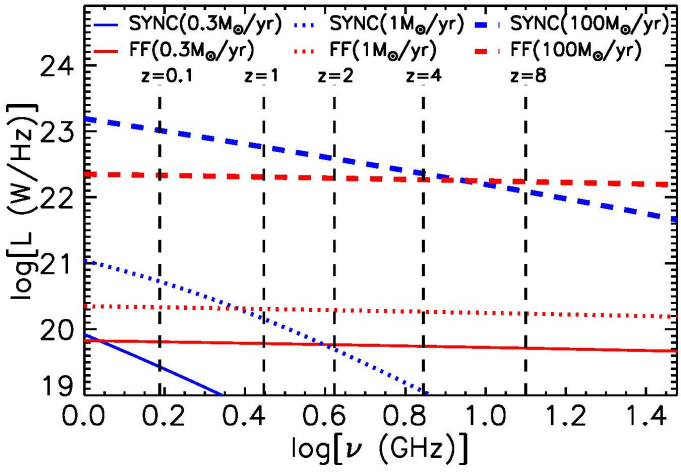

Fig. 2: Synchrotron and free-free luminosity of star-forming galaxies as a function of frequency (in the source frame) for 3 values of the SFR (0.3, 1 and 100 $M_\odot\,\mathrm{yr}^{-1}$). The vertical dashed lines show the source-frame frequency corresponding to 1.4 GHz in the observer's frame. Objects with low SFRs are expected to be detectable via their free-free emission, particularly at high z.

stellar Initial Mass Function, of the metallicity and of the star formation history. Mancuso et al. (2015) have slightly modified the relation including a steepening of the synchrotron spectrum by $\Delta\alpha = 0.5$ above a break frequency of 20 GHz, to take into account electron ageing effects (Banday & Wolfendale, 1991). The SFR-synchrotron luminosity relation then writes:

$$\bar{L}_{\mathrm{sync}} \simeq 1.9 \times 10^{21} \left(\frac{\mathrm{SFR}}{\mathrm{M}_\odot \mathrm{yr}^{-1}}\right) \left(\frac{\nu}{\mathrm{GHz}}\right)^{-0.85} \left[1 + \left(\frac{\nu}{20\mathrm{GHz}}\right)^{0.5}\right]^{-1} \mathrm{W\,Hz}^{-1}. \quad (1)$$

This calibration implies a linear relation between L_{sync} and SFR at all luminosities. However, it has long been suggested that the synchrotron radiation from low SFR galaxies is somewhat suppressed (Klein et al., 1984; Chi & Wolfendale, 1990; Price & Duric, 1992), although this view was controversial (Condon, 1992).

A convincing argument in this direction was made by Bell (2003). He pointed out that the FIR emission traces most of the SFR in luminous star-forming galaxies but only a minor fraction of it in low luminosity ones, as demonstrated by the fact that they are mostly blue, implying that only a minor fraction of the light from young stars is absorbed by dust. Nevertheless the FIR to radio luminosity ratio is similar for the two galaxy groups, implying that the radio emission from low-luminosity galaxies is substantially suppressed, compared to brighter galaxies. A plausible physical reason for the suppression of synchrotron emission of low luminosity galaxies is that they are unable to confine relativistic electrons, which can then escape into the intergalactic medium before releasing their energy via synchrotron emission.

A direct test of the L_{sync} vs SFR relation can be made comparing the observationally determined local SFR function (Mancuso et al., 2015; Aversa et al., 2015) with the local radio luminosity function (Mauch & Sadler, 2007). To reconcile the

SFR function with the radio LF we need to assume that the $L_{\rm sync}$/SFR ratio declines at low SFRs. Following Massardi et al. (2010), Mancuso et al. (2015) adopted a relation of the form:

$$L_{\rm sync}(\nu) = \frac{L_{\star,{\rm sync}}(\nu)}{\left(L_{\star,{\rm sync}}/\bar{L}_{\rm sync}\right)^{\beta} + \left(L_{\star,{\rm sync}}/\bar{L}_{\rm sync}\right)}, \qquad (2)$$

where $\bar{L}_{\rm sync}$ is given by eq. (1) and $\beta = 3$. This equation converges to the Murphy et al. (2011) relation for $\bar{L}_{\rm sync} \gg L_{\star,{\rm sync}} = 0.886\bar{L}_{\rm sync}({\rm SFR} = 1\,M_\odot\,{\rm yr}^{-1})$. At 1.4 GHz, $L_{\star,{\rm sync}} \simeq 10^{28}\,{\rm erg\,s^{-1}\,Hz^{-1}}$. The agreement at high luminosities is recovered taking into account a dispersion of $\sigma_{\rm radio} = 0.4$ dex around the mean $L_{\rm radio}$–SFR relation.

The suppression of the synchrotron luminosity of low-SFR galaxies make their free-free emission detectable over a broader frequency range, particularly at high z, as illustrated by Fig. 2. The relation between SFR and *free-free emission* derived by Murphy et al. (2012), again using the Starburst99 stellar population models, writes:

$$L_{\rm ff} = 2.18\times10^{20}\left(\frac{\rm SFR}{M_\odot{\rm yr}^{-1}}\right)\left(\frac{T}{10^4\,{\rm K}}\right)^{0.45}\nu_{\rm GHz}^{-0.1}\,\exp\left(-\frac{h\nu}{k{\rm T}}\right){\rm W\,Hz^{-1}}, \qquad (3)$$

where T is the temperature of the emitting plasma, h is the Planck constant and k is the Boltzmann constant. The free-free luminosity at given SFR and for ${\rm T} = 10^4$ K has thus an amplitude at 1 GHz about a factor of 7 lower than the synchrotron luminosity. However its flatter slope, extending up to $\nu \sim kT/h \simeq 2.1\times10^{14}$ Hz, i.e. up to the optical band, implies $L_{\rm ff} > L_{\rm sync}$ for $\nu \gtrsim 10$ GHz, if indeed the synchrotron spectrum steepens above $\gtrsim 20$ GHz.

Since the most extreme starbursts at high redshifts reach SFRs of thousands $M_\odot{\rm yr}^{-1}$, the highest luminosities at 1.4 GHz due to star formation are of several times $10^{24}\,{\rm W\,Hz^{-1}}$ consistent with the local luminosity function of Mauch & Sadler (2007).

The tight relationship between radio and FIR luminosity is exploited as one of the main indicators to separate radio AGNs from SFGs in deep radio surveys: excess radio emission with respect to that expected given the SFR is attributed to nuclear radio activity, leading to a classification as radio AGN. The correlation is usually parameterized through the so-called q parameter (Helou et al., 1985):

$$q_{\rm FIR} = \log\left(\frac{L_{\rm FIR}[{\rm W}]}{3.75\times10^{12}}\right) - \log\left(L_{1.4\,{\rm GHz}}[{\rm W\,Hz^{-1}}]\right), \qquad (4)$$

where $L_{\rm FIR}$ is the FIR luminosity integrated from rest-frame 42 to 122 μm and $L_{1.4\,{\rm GHz}}$ is the rest-frame 1.4 GHz luminosity.

A better choice would be $q_{\rm IR}$, where the FIR luminosity is replaced by the total (8–1000 μm) IR luminosity. However, to compute $L_{\rm IR}$ we need *Herschel* data, which are available for a small fraction of faint radio sources. Frequently we need to make do with *Spitzer* 24 μm data, a very uncertain proxy of the FIR/IR luminosity. Also, the dividing line between SFGs and radio-excess sources (RL AGNs) is somewhat arbitrary.

Several models predict that the synchrotron emission is suppressed at high z because of the energy losses of relativistic electrons due to inverse Compton scattering

off the Cosmic Microwave Background photons, whose energy density increases as $(1+z)^4$ (e.g., Norris et al., 2013). On the contrary, Magnelli et al. (2015), based on FIR and radio observations of the most extensively studied extragalactic fields (GOODS-N, GOODS-S, ECDFS, and COSMOS), reported evidence of a weak redshift evolution of the parameter $q_{\rm FIR}$, in the sense of an increasing radio excess with increasing redshift. They found:

$$q_{\rm FIR} = (2.35 \pm 0.08) \times (1+z)^{\alpha_M}, \tag{5}$$

with $\alpha_M = -0.12 \pm 0.04$. The weak but statistically significant trend of $q_{\rm FIR}$ with redshift has been recently confirmed by Calistro Rivera et al. (2017) up to $z \simeq 2.5$ and by Delhaize et al. (2017) up to $z \simeq 5$. Molnár et al. (2018) repeated the analysis on the Delhaize et al. (2017) sample for disc- and spheroid-dominated galaxies separately. They measured very little change in $q_{\rm FIR}$ up to $z \simeq 1$–1.5 for disc-dominated galaxies and an increased radio excess with increasing z at $z \gtrsim 0.8$ for spheroid-dominated galaxies. They suggested that this may hint at some residual AGN activity in the latter objects.

The evolution of $q_{\rm FIR}$ reported by Magnelli et al. (2015) implies an increase with redshift of the $L_{\rm synch}$/SFR ratio:

$$\log[L_{\rm synch,1.4GHz}(z)] = \log[L_{\rm synch,1.4GHz}(0)] + 2.35[1-(1+z)^{-0.12}]. \tag{6}$$

This is in contradiction with expectations from inverse Compton cooling of relativistic electrons at high redshifts. On the other hand, a decrease in $q_{\rm FIR}$ with redshift was expected by some of the most up-to-date theoretical models (e.g., Lacki et al., 2010; Lacki & Thompson, 2010; Schleicher & Beck, 2013) because of the increase with redshift of the SFR surface density and of the gas density that may better confine relativistic electrons; the magnetic field may also be amplified.

However, the precise mechanism accounting for the radio–FIR correlation, including the evolution of $q_{\rm FIR}$ is not well understood yet. A direct test of the $L_{\rm sync}$–SFR relation, made comparing the observational determinations of the SFR function and of the radio luminosity function, now available up to high redshifts, has been carried out by Bonato et al. (2017).

Determinations of the SFR function need to take into account both the unobscured and the dust-obscured star formation. At high SFRs, the star formation is almost completely dust-obscured and can be measured via FIR/sub-mm observations. At low SFR, most star-formation is unobscured and can be measured via optical/UV observations both in the continuum or in emission lines (primarily Lyα and Hα; Cai et al., 2014; Aversa et al., 2015).

The radio luminosity functions at 1.4 GHz derived from the SFR functions via eqs. (2) and (3) were found to match quite well the observational determinations available at several redshifts, up to $z \simeq 5$. The fits were similarly good both with and without the weak evolution of $q_{\rm FIR}$ found by Magnelli et al. (2015). The evolution is preferred by data at the highest redshifts, which however have larger uncertainties.

Stronger support to the case for an increase with z of the $L_{\rm synch}$/SFR ratio is provided by the source counts: without evolution the predicted counts lie below the observational determinations while the evolution by Magnelli et al. (2015) leads to good agreement. The counts turn out to be quite sensitive to the evolution of the $L_{\rm synch}$/SFR ratio: a slightly stronger evolution, with the coefficients of the Magnelli

relation at their $1\,\sigma$ limits, yields counts at hundreds of μJy flux densities at the upper limits of observational determinations.

5 Identification of the faint (sub-mJy) population

Determining the nature of the sub-mJy radio sources requires optical/IR spectroscopy to measure the redshift, hence the luminosity, and to classify them as SFGs or AGNs. These objects however are very faint in the optical. For example, the median R magnitude for the Extended Chandra Deep Field-South (E-CDFS) VLA sample, which reaches $S_{1.4\,\mathrm{GHz}} \simeq 32.5\,\mu$Jy, is ~ 23; and this refers only to sources detected in the R band, while $\sim 20\%$ of the objects have only an IR counterpart (Bonzini et al., 2012).

Getting spectra for such faint sources is very time consuming (prohibitively so for the very faint tail) but can in principle be done. Even if we had optical spectra for all the E-CDFS sources, for faint counterparts one can only see a couple of lines. This is enough to get a redshift but not to properly classify the objects (Padovani, 2016). The classification thus turns out to be quite complex and has to resort to indicators of varying effectiveness and reliability.

The X-ray emission is a powerful indicator of nuclear activity, but the mere presence of an active nucleus does not necessarily imply that it is contributing to the radio emission. If nuclear activity is detected but the radio luminosity is consistent with the expectation from the SFR of the host galaxy, the source is classified as a radio quiet (RQ) AGN. This classification criterion has at least a couple of limitations. First, the minimum luminosity detectable by X-ray surveys increases with increasing redshift and even the deepest currently available surveys miss a large fraction of high-z AGNs (cf. Fig. 1 of Bonzini et al., 2013). Second, X-ray luminosities of up to $\sim 10^{42}\,\mathrm{erg\,s^{-1}}$ can be accounted for by processes related to star formation and this prevents a firm identification of weak nuclear activity.

Whenever X-ray data are missing, the identification of RQ AGNs can be made using deep observations with the Spitzer Infrared Array Camera (IRAC) at 3.6, 4.5, 5.8 and $8\,\mu$m. Different extragalactic sources occupy somewhat different regions in the diagram of the $S_{8.0}/S_{4.5}$ versus $S_{5.8}/S_{3.6}$ ratios (Donley et al., 2012, and references therein). This is because the AGN emission can heat up the surrounding dust that re-emits this energy in the mid-IR. If the AGN is sufficiently luminous compared to its host galaxy, the emission from the dust heated by it (which is warmer than that heated by stars) can produce a power-law thermal continuum across the four IRAC bands. Sources with this spectral shape occupy a specific region in the IRAC colour–colour diagram, the so-called Lacy wedge (Lacy et al., 2004). The completeness of this selection method is therefore high ($\sim 75\%$) at $L_x \geq 10^{44}\,\mathrm{erg\,s^{-1}}$, but relatively low ($\lesssim 20\%$) for $L_x \leq 10^{43}\,\mathrm{erg\,s^{-1}}$. The IRAC selection appears also to be incomplete to radio galaxies (Donley et al., 2012) and also easily misses Type 2 Seyfert galaxies. Nevertheless, the mid-IR (MIR) selection is very important since it identifies also heavily obscured AGNs (provided that they are not hosted by a particularly bright galaxy), many of which are missed even by deep X-ray surveys (Donley et al., 2012).

In short, to classify faint radio sources:

- one first selects radio AGNs using a variant of the IR–radio correlation;

- then radio AGNs are separated from SFGs using X-ray observations;
- next, the IRAC colour-colour diagram or SED (spectral energy distribution) fitting decomposition (Delvecchio et al., 2017) are used to recover (RQ) AGNs missed by the X-ray criterion;
- finally, other indicators (radio spectra, radio morphology, optical lines, optical photometry, ...), if available, are applied to catch possible outliers.

The classification work has demonstrated that early attempts overestimated the fraction of SFGs among sub-mJy sources. This was caused by a selection effect: SFGs have higher optical to radio luminosity ratios than RL AGNs and therefore are over-represented in samples identified through magnitude limited optical imaging. Only $\simeq 44\%$ of the complete sample of sub-mm radio sources studied by Windhorst et al. (1985) were optically identified, and $\simeq 70\%$ of these were found to be galaxies, mostly blue (star forming). But this fact did not warrant that the majority of sub-mJy sources are star-forming galaxies, as assumed by several authors.

The most recent, extensive study of the composition of the faint radio population (Smolčić et al., 2017) was carried out on the sample from the Very Large Array Cosmic Evolution Survey (VLA-COSMOS) 3 GHz Large Project. The survey covers a $2.6\,\mathrm{deg}^2$ area with a mean rms of $\sim 2.3\,\mu$Jy/beam. The radio data were combined with optical, near-infrared (UltraVISTA), and mid-infrared (Spitzer/IRAC) data, as well as X-ray data (Chandra). This yielded counterparts for $\simeq 93\%$ of the total radio sample of 10,830 sources, reaching out to $z \lesssim 6$.

Smolčić et al. (2017) first selected moderate-to-high radiative luminosity AGN (HLAGN) by using a combination of X-ray ($L_\mathrm{X} > 10^{42}$ erg s^{-1}), IRAC colour-colour and SED-fitting criteria. About 30% of the HLAGN show a $> 3\sigma$ radio-excess in $\log(L_{1.4\mathrm{GHz}}/\mathrm{SFR})$ diagram, while the remaining $\sim$70% have a radio luminosity consistent (within $\pm 3\sigma$) with the star-formation rates in their host galaxies.

SFGs were selected based on evidence of star formation (either blue and green near-UV (NUV)-optical colours, or red colours but with a detection by *Herschel*) and excluding objects with $> 3\sigma$ radio-excess. Finally, low-to-moderate radiative luminosity AGN (MLAGN) were drawn from the sample remaining after exclusion of the HLAGN, selecting sources with $> 3\sigma$ radio-excess (radio-excess-MLAGN) and sources with red NUV-optical colours and no *Herschel* detection (quiescent-MLAGN).

The contribution of MLAGN to the 3 GHz source counts decreases from about 75% at $S_{3\mathrm{GHz}} \sim 400-800\,\mu$Jy to about 50% at $S_{3\mathrm{GHz}} \sim 100-400\,\mu$Jy, and to $\simeq 20\%$ at $S_{3\mathrm{GHz}} \sim 50\,\mu$Jy. In the same flux density interval, the fraction of SFGs increases from $\simeq 10\%$ ($S_{3\mathrm{GHz}} \sim 400 - 800\ \mu$Jy) to $\simeq 60\%$ ($S_{3\mathrm{GHz}} \sim 50\ \mu$Jy). The fraction of HLAGN remains approximately constant, at 20-30%. Hence the combined AGN sample (MLAGN and HLAGN) dominates at $S_{3\mathrm{GHz}} \gtrsim 100\ \mu$Jy while SFGs take over at lower flux densities.

The above definitions of MLAGNs and HLAGN imply that a fraction of them have radio emission consistent with that expected from star formation. Separating the sources into two groups, with and without $> 3\sigma$ radio excess, Smolčić et al. (2017) found that the fraction of sources whose radio luminosity can be accounted for by star formation increases from about 10% at $S_{1.4\mathrm{GHz}} \sim 700 - 1000\ \mu$Jy to $\sim 50\%$ at $S_{1.4\mathrm{GHz}} \sim 200, \mu$Jy, to $\sim 85\%$ at $S_{1.4\mathrm{GHz}} \sim 50\ \mu$Jy.

Similar results, once we take into account the differences in the selection criteria, were reported by Bonzini et al. (2013) who classified the sources detected in the 1.4 GHz VLA survey of the Extended Chandra Deep Field-South (E-CDFS). The VLA/E-CDFS survey covered an area of $0.3\,\mathrm{deg}^2$ reaching a flux density limit of $\simeq 32\,\mu$Jy.

6 Radio quiet (RQ) AGNs: a new radio source population?

Although the discovery of quasi stellar objects (QSOs)[4] sprang from the optical identification and redshift measurement of a powerful radio source (3C273; Schmidt, 1963) and the first QSOs were radio-selected, it became clear relatively soon (Sandage, 1965) that the majority of QSOs are not radio loud (RL); they are usually referred to as radio quiet (RQ). Several follow-up surveys at radio frequencies of optically selected QSOs, reviewed by Stern et al. (2000), typically detected between 10% and 40% of them.

The fraction of radio-detected QSOs increased with the depth of radio surveys, suggesting that RQ AGNs are perhaps only "radio-faint" As we have seen, identifications of sub-mJy radio sources have revealed the presence of a substantial fraction RQ AGNs. Evidence of nuclear activity in these sources comes from other bands (e.g. optical, mid-infrared, X-ray) so that the link between the nuclear activity and the radio emission is unclear and is still being hotly debated.

Many papers have addressed the question: is there a continuity between RL and RQ AGNs, so that the latter simply populate the low radio luminosity tail of the AGN distribution or RQ and RL AGNs are two totally distinct populations, at least as far as radio properties are concerned?

Kellermann et al. (1989) reported a bimodal distribution of the radio flux density of QSOs from the optically selected Palomar Bright Quasar survey observed with the Very Large Array (VLA) at 5 GHz. The bimodality suggests that two distinct physical processes are present, with one process being significantly more powerful than the other for different QSO classes. Deep Expanded VLA (EVLA) observations at 6 GHz with nearly complete (97%) radio detections in a volume-limited colour-selected sample of 179 QSOs (Kimball et al., 2011) have shown that the radio luminosity function (LF) can be explained as a superposition of two populations: QSO radio sources with $\log(L_{6\,\mathrm{GHz}}/\mathrm{erg\,s^{-1}\,Hz^{-1}}) > 30$ are powered primarily by nuclear activity, while those with lower 6 GHz luminosity are dominated by star formation in the QSO host galaxies. Support to this conclusion was provided by Condon et al. (2013) who used the 1.4 GHz NRAO VLA Sky Survey (NVSS) to study radio sources in two colour-selected QSO samples.

A careful analysis of the dichotomy in the radio loudness distribution of QSOs was carried out by Baloković et al. (2012) by modeling their radio emission and various selection effects using a Monte Carlo approach. The resulting simulated samples were compared to a fiducial sample of 8300 QSOs drawn from the seventh data release of the Sloan Digital Sky Survey (SDSS DR7) Quasar Catalog and combined with radio observations from the Faint Images of the Radio Sky at Twenty cm (FIRST) survey. Their results indicated that the SDSS–FIRST sample is best described by a

[4]Throughout this paper we will use preferentially the term AGN to refer to sources powered by nuclear activity. However, AGNs will also be referred to as "QSOs" or "quasars" when these terms are used in the cited papers.

radio loudness distribution consisting of two components, with $(12 \pm 1)\%$ of sources in the radio-loud component. The evidence for bimodality was however found to be not strong.

Based on their study of the Extended Chandra Deep Field-South (E-CDFS) VLA sample Padovani et al. (2015) concluded that RQ and RL QSOs are two totally distinct populations, characterized by very different evolutions, luminosity functions, and Eddington ratios. The radio power of RQ AGNs evolves similarly to star-forming galaxies, consistent with their radio emission being powered by star formation. This conclusion was confirmed by the study of Bonzini et al. (2015) who used deep *Herschel* photometry to determine the FIR luminosity, hence the SFR, of E-CDFS galaxies.

On the other hand, Lacy et al. (2001) and Cirasuolo et al. (2003) found a continuous distribution of radio-to-optical flux ratios, without a minimum between those of RL and RQ AGNs (but see Ivezić et al., 2002, 2004, for a different interpretation). This view was corroborated by Barvainis et al. (2005) who, through a study of radio variability across a broad range of radio power, from quiet to loud, came to the conclusion that "... the radio emission from radio-quiet quasars originates in a compact structure intimately associated with the active nucleus. The alternative hypothesis, that the emission from radio-weak quasars is from a starburst, is ruled out."

A similar conclusion was reached by Bonchi et al. (2013) studying the dependence of the nuclear radio (1.4 GHz) luminosity on both the 2–10 keV X-ray and the host-galaxy K-band luminosities for a complete sample of 1268 X-ray-selected AGNs. No evidence of bimodality in the radio luminosity distribution was found. This continuity is consistent with a nuclear origin of the radio emission for both RQ and RL AGNs.

White et al. (2015) used a combination of optical and near-infrared photometry to select, from the VISTA Deep Extragalactic Observations (VIDEO) survey, a sample of 74 objects that can be confidently classified as QSOs ('Gold candidate quasar sample') over $1\,\mathrm{deg}^2$. By comparing the radio flux-density distribution for these QSOs with that for a control sample of galaxies matched in redshift and stellar mass, and by estimating the star formation rate, they found that the QSOs have excess radio flux when assuming the most reasonable values of black hole masses. This result was interpreted as indicating "that accretion is the primary origin of the quasars' total radio emission."

Direct evidence for a nuclear origin of the radio emission from RQ AGNs were provided via high angular resolution observations by Giroletti & Panessa (2009), Guidetti et al. (2013), Jackson et al. (2015) and Herrera Ruiz et al. (2016). Zakamska et al. (2016) assembled two samples of optically obscured or unobscured AGNs for which the host star formation rates (SFRs) could be estimated or constrained with infrared spectroscopy and photometry from *Spitzer* and *Herschel*. The SFRs were found to be insufficient, by an order of magnitude, to explain the observed radio emission derived by cross–matching the samples with the FIRST survey catalog. They concluded that, although RQ AGNs in their samples lie close to the infrared/radio correlation characteristic of the star-forming galaxies, both their infrared emission and their radio emission are dominated by the nuclear activity, not by the host galaxy.

It is clear from the above review that the radio properties of RQ AGNs are not yet

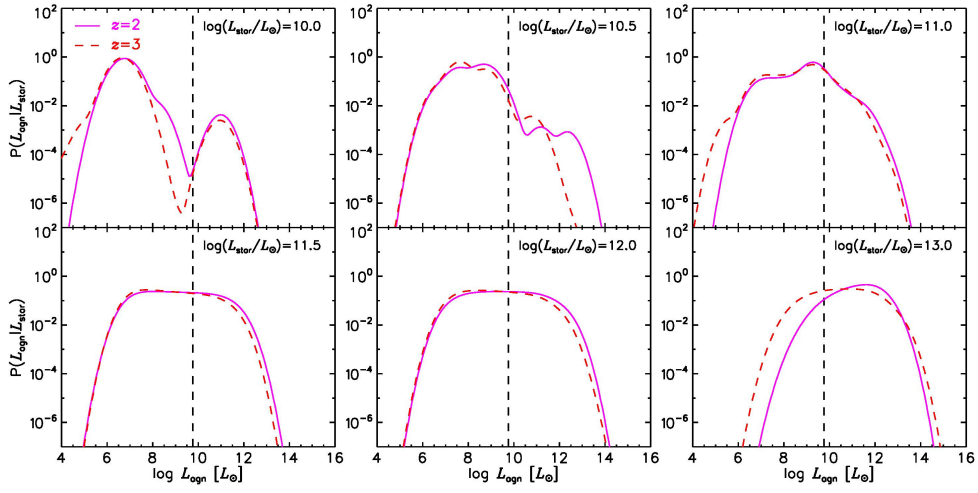

Fig. 3: Probability that a star-forming proto-spheroidal galaxy with luminosity $L_{\rm star}$ at redshift $z = 2$ or $z = 3$ (solid and dashed lines, respectively) hosts an AGN with luminosity $L_{\rm agn}$ within $d \log L_{\rm agn}$ [eq. (7)]. $L_{\rm star}$ is a measure of the SFR [eq. (9)]. The vertical dashed lines correspond to $L_{\rm agn} = 22.4 \times 10^{42}\,{\rm erg\,s^{-1}} = 5.8 \times 10^9\,L_\odot$, where $10^{42}\,{\rm erg\,s^{-1}}$ is the minimum X-ray luminosity of E-CDFS VLA sources classified as RQ AGNs by Bonzini et al. (2013) and 22.4 is the bolometric correction adopted by Chen et al. (2013).

well understood. Observational indications both of a nuclear and of a star formation origin have been reported. The two mechanisms frequently co-exist and it is unclear which is the dominant one, in a statistical sense. The galaxy-AGN co-evolution model by Cai et al. (2013), extended by Cai et al. (2014), Bonato et al. (2014) and Mancuso et al. (2015), allows us to investigate whether or not the amount of star formation of AGN hosts is sufficient to explain the counts and the radio luminosity functions of RQ AGNs associated to sub-mJy radio sources.

The model comprises two populations of star-forming galaxies, late-types that are dominating the cosmic star formation rates at $z \lesssim 1.5$, and proto-spheroids, that formed the bulk of their stars at higher redshifts in a relatively short time, $\lesssim 1\,{\rm Gyr}$, at $z > 1$–1.5.

The formation and evolution of proto-spheroidal galaxies is linked to the formation of massive halos. The baryonic gas falling into the halo potential wells is shock-heated to the virial temperature and then cools down giving rise to star formation. At the same time it loses angular momentum, e.g. by effect of the radiation drag, and flows towards the central regions at a rate proportional to the SFR. It is temporarily stored in a reservoir/proto-torus from which it flows into the supermassive black hole at the rate allowed by the viscous dissipation of the angular momentum. A small fraction of the emitted power comes out in mechanical form. In massive objects, this AGN feedback exceeds that from supernovae (also taken into account by the model) and the gravitational binding energy of the gas. The gas is thus eventually swept out of the potential well. Consequently both the star formation and the gas supply to the reservoir are halted. The nuclear activity however continues until the reservoir is depleted.

These processes are governed by a set of equations, laid down in the Appendix

of Cai et al. (2013). The formalism has allowed the calculation of the evolution with galactic age of the SFR and of the AGN bolometric luminosity for any galaxy halo mass and redshift. We can then compute the probability that a galaxy of given redshift and given SFR hosts an AGN with X-ray luminosity $L_{\rm X} > 10^{42}\,{\rm erg\,s^{-1}}$ and is therefore classified as a RQ AGN.

The probability that a galaxy with total luminosity due to star formation $L_{\rm star}$ at redshift z hosts an AGN with bolometric luminosity $L_{\rm agn}$ within $d\log L_{\rm agn}$, hence with total luminosity $L_{\rm tot} = L_{\rm star} + L_{\rm agn}$, is:

$$P_{\rm protosph}(L_{\rm agn}|L_{\rm star},z) \equiv \frac{\Phi_{\rm agn}[L_{\rm agn}|L_{\rm tot},z]}{\int_{\log L_{\rm agn,min}}^{\log L_{\rm agn,max}} \Phi_{\rm agn}[L_{\rm agn}|L_{\rm tot},z]d\log L_{\rm agn}}, \qquad (7)$$

where $\Phi_{\rm agn}(L_{\rm agn}|L_{\rm tot},z)$ is the conditional AGN luminosity function per unit $d\log L_{\rm agn}$, derived by Bonato et al. (2014):

$$\begin{aligned}\Phi_{\rm agn}(L_{\rm agn}|L_{\rm tot},z) &= \int_{M_{\rm min}}^{M_{\rm max}} dM_{\rm vir} \\ &\times \int_{z}^{z_{\rm max}} dz_{\rm vir} \left|\frac{dt_{\rm vir}}{dz_{\rm vir}}\right| \frac{dN_{\rm ST}}{dt_{\rm vir}}(M_{\rm vir},z_{\rm vir}) \frac{1}{2\pi\sigma_{\rm star}\sigma_{\rm agn}} \\ &\times \frac{L_{\rm tot}}{L_{\rm tot}-L_{\rm agn}} \exp\{-[\log(L_{\rm tot}-L_{\rm agn}) - \log\bar{L}_{\rm star}]^2/2\sigma_{\rm star}^2\} \\ &\times \exp[-(\log L_{\rm agn} - \log\bar{L}_{\rm agn})^2/2\sigma_{\rm agn}^2]. \end{aligned} \qquad (8)$$

In the above equation $\bar{L}_{\rm star} = \bar{L}_{\rm star}(z|M_{\rm vir},z_{\rm vir})$ and $\bar{L}_{\rm agn} = \bar{L}_{\rm agn}(z|M_{\rm vir},z_{\rm vir})$ are the redshift-dependent mean starburst and AGN luminosities at given halo mass, $M_{\rm vir}$, and virialization redshift, $z_{\rm vir}$, respectively, and $\sigma_{\rm star}$ and $\sigma_{\rm agn}$ are the corresponding dispersions for which we have adopted the values derived by Cai et al. (2013): $\sigma_{\rm star} = 0.1$ and $\sigma_{\rm agn} = 0.35$. $dN_{\rm ST}/dt$ is the dark matter halo mass function (Sheth & Tormen, 1999).

Examples of the probability distributions given by eq. (7) are shown in Fig. 3 for two values of the redshift ($z = 2$ and $z = 3$) and for several values of $L_{\rm star}$, which is a measure of the SFR:

$$\log\left(\frac{L_{\rm star}}{L_\odot}\right) = \log\left(\frac{\rm SFR}{M_\odot\ {\rm yr}^{-1}}\right) + 9.892. \qquad (9)$$

As mentioned above, the local luminosity function by Mauch & Sadler (2007) can be reproduced adopting a Gaussian distribution of the radio luminosities with a dispersion $\sigma_{\rm radio} = 0.4$ dex around the mean $L_{\rm radio}$–SFR relation:

$$\Phi_{\rm radio}(L_\nu|{\rm SFR}) = \frac{\phi({\rm SFR})}{\sigma_{\log L}\sqrt{2\pi}} \exp\left\{-\frac{1}{2}\left[\frac{\log[L_\nu/\bar{L}_\nu({\rm SFR})]}{\sigma_{\log L}}\right]^2\right\} \frac{d\log({\rm SFR})}{d\log(L_\nu)}, \qquad (10)$$

where $\bar{L}_\nu({\rm SFR}) = L_{\rm sync}(\nu|{\rm SFR}) + L_{\rm ff}(\nu|{\rm SFR})$ and $\sigma_{\log(L)} = 0.4$.

The contribution of proto-spheroidal galaxies to the radio LF of RQ AGNs is then obtained multiplying the distribution of radio luminosities of galaxies at fixed SFR [eq. (10)] by the probability that a galaxy with such SFR (or with the corresponding total luminosity due to star formation, $L_{\rm star}$), at redshift z hosts an AGN

with bolometric luminosity $L_{\rm agn} > 22.4 \times 10^{42}\,{\rm erg\,s^{-1}}$. Here 22.4 is the bolometric correction (Chen et al., 2013) and $10^{42}\,{\rm erg\,s^{-1}}$ is the minimum X-ray luminosity of sources classified as RQ AGNs by Bonzini et al. (2013). This probability is computed integrating eq. (7) over $d\log L_{\rm agn}$.

As for late-type galaxies, Bonato et al. (2014) argued that the probability of finding a RQ AGN with $L_{\rm X} > 10^{42}\,{\rm erg\,s^{-1}}$ inside a star–forming galaxy with a given SFR (or associated luminosity $L_{\rm star}$) can be be described by a Gaussian distribution with a dispersion $\sigma_{\rm lt} = 0.69\,{\rm dex}$ around the mean $\bar{L}_{\rm X}({\rm SFR})$:

$$\log\left(\frac{\bar{L}_{\rm X}}{{\rm erg\,s^{-1}}}\right) = 30.17 + 1.05\log\left(\frac{L_{\rm IR}}{L_\odot}\right). \tag{11}$$

The wanted probability is then:

$$P_{\rm lt}(L_\nu) = \frac{1}{\sigma_{\rm lt}\sqrt{2\pi}}\exp\left\{-\frac{1}{2}\left[\frac{\log(L_{\rm X}/\bar{L}_{\rm X}({\rm SFR}))}{\sigma_{\rm lt}}\right]^2\right\}\frac{d\log({\rm SFR})}{d\log(\bar{L}_\nu)}. \tag{12}$$

The contribution of late-type galaxies to the radio LF of RQ AGNs then follows as in the case of proto-spheroids.

The resulting radio luminosity functions of RQ AGNs turn out to be in good agreement with observational determinations, available at several redshifts (Bonato et al., 2017, and paper in preparation). This means that the data are consistent with the hypothesis that the radio emission associated to star formation can account for the statistical properties (number counts, redshift-dependent luminosity functions) of faint radio sources not associated to RL AGNs, with and without nuclear activity detectable in other wavebands. However, this does not mean that the radio emission of RQ AGNs must be negligible. The uncertainties are large enough to leave room for significant, although not dominant, contributions from these objects.

In summary, recent surveys of the faint radio sky are playing an important role in a variety of astrophysical topics, including the understanding of the cosmic star formation history, the galaxy evolution, the existence of powerful jets, and the radio emission in RQ AGNs.

Assessing the nature of sub-mJy radio sources took more than thirty years because radio surveys were exploring galaxies fainter than those accessible in other wavebands. Now it is well established that below $S_{1.4{\rm GHz}} \simeq 0.1\,{\rm mJy}$ the radio sky is dominated by SFGs. As we will see in the next section, the Square Kilometre Array (SKA) that will reach flux limits orders of magnitude fainter than is currently possible, and over large areas, will boost the potential of radio astronomical observations for extragalactic studies related to star formation and galaxy and AGN evolution.

Radio observations are unaffected by absorption, which means, for example, that they can dig out the most extremely dust-enshrouded star-forming regions and are sensitive to all types of AGN, irrespective of obscuration and orientation (i.e., Type 1s and Type 2s). But the full exploitation of the SKA potential requires synergies with other multi-wavelength astronomical such as the Advanced Telescope for High ENergy Astrophysics (ATHENA; Barcons et al., 2015), the Wide Field Infrared Survey Telescope (WFIRST; Spergel et al., 2015), the Large Synoptic Survey Telescope (LSST; LSST Science Collaboration et al., 2017), the European Extremely Large Telescope (E-ELT; Liske et al., 2012), the James Webb Space Telescope (JWST; Gardner, 2012; Greenhouse, 2015), and the Space Infrared Telescope for Cosmology and Astrophysics (SPICA; Nakagawa et al., 2017).

7 The SKA and the study of the cosmic star-formation history

The SKA (see, e.g., Combes, 2015; Grainge et al., 2017)[5] is a new technology radio-telescope array, with one square kilometre collecting surface, orders of magnitude more sensitive and rapid in sky surveys than present instruments.

The SKA comprises two separate interferometric arrays. In 2012, it was decided that they will be hosted by two desert sites, chosen to minimize terrestrial interference, in different continents. The SKA-low telescope, that will operate between frequencies of 50 and 350 MHz, will be deployed at the Murchison Radio Astronomy Observatory, Australia. At the end of Phase 1 it will incorporate a total of 131,072 antennas, grouped into 512 stations of 256 antennas each. The majority (296) of these stations will be located in a "core" area; the remaining 216 will be deployed along three spiral arms to give a maximum baseline of 65 km.

The SKA-mid telescope will operate between 350 MHz and 24 GHz and will be located in the Karoo desert in South Africa. At the end of Phase 1 (SKA1) it will be made up of 133 antennas with 15-m diameter, plus 64 antennas of 13.5-m diameter being built for the MeerKAT telescope. Again, there will be a central core of antennas and three spiral arms allowing a maximum baseline of 156 km. In Phase 2 (SKA2) the number of SKA-mid dishes will be increased to ~ 2000 across 3500 km of Southern Africa and a major expansion of SKA1-Low across Western Australia is also foreseen.

A key feature of the SKA is that traditional dish radio telescope designs, which will be used in the high frequency component, will be complemented with aperture arrays. These are made by large numbers of small, fixed antenna elements coupled to appropriate receiver systems which can be arranged in a regular or random pattern on the ground. A signal "beam" (or field-of-view, FoV) is formed and steered by combining all the received signals after appropriate time delays have been introduced to align the phases of the signals coming from a particular direction. By simultaneously using different sets of timing delays, this "beam forming" can be repeated many times to create multiple independent beams. This FoV expansion technology will allow instantaneous imaging of multiple sky regions simultaneously, massively increasing the telescope survey speed.

The number of useful beams produced, or total FoV, is essentially limited by signal processing, data communications and computing capacity. With 8 independent beams, the FoV is of $1\,\mathrm{deg}^2$ at 1.4 GHz (21 cm) and could, in principle, be extended by up to a factor of 100. For comparison, the Hubble Space Telescope (HST) FoV is $\sim 1\,\mathrm{arcmin}^2$ and the ALMA FoV is $\sim 0.25\,\mathrm{arcmin}^2$.

The angular resolution also depends on frequency: it is higher/poorer at higher/lower frequencies. The Phase 1 goal is to achieve a resolution of ~ 0.2 arcsec at 1.4 GHz. In Phase 2 the resolution at this frequency will improve to 0.01 arcsec with baselines of ~ 3000 km.

The construction of the SKA will start in 2018. The SKA1 instruments are expected to be in place on 2024. The construction cost cap for this phase, inflation adjusted, is of 674.1 million euro. The SKA2 is expected to start in the mid-2020's. The total estimated SKA construction cost is about 1.5 billion euros.

The SKA is a world-wide project. Ten countries (Australia, Canada, China,

[5] See also
`www.skatelescope.org/wp-content/uploads/2017/02/SKA-Community-Briefing-18Jan2017.pdf`

India, Italy, Netherlands, New Zealand, South Africa, Sweden and UK) are currently members of the SKA organization. Several other countries (France, Germany, Japan, Korea, Malta, Portugal, Spain, Switzerland, USA) have expressed interest in joining.

The three radio telescopes that have been built on the two selected SKA sites are called the SKA precursors, to be included in the final instrument. They are the Murchison Widefield Array (MWA) and ASKAP in Australia, and MeerKAT in South Africa. The MWA is a low-frequency radio telescope operating between 80 and 300 MHz. It is performing large surveys of the entire Southern sky and acquiring deep observations on targeted regions.

ASKAP is designed to be a high speed survey instrument with high dynamic range. It has a total collecting area of approximately $4,000\,\mathrm{m}^2$, from 36 antennas each 12 m in diameter; covers the frequency range from 700 MHz to 1.8 GHz; operates with 36 independent beams, each of about $1\,\mathrm{deg}^2$, yielding a total FoV of $30\,\mathrm{deg}^2$ at 1.4 GHz. The ASKAP Early Science Program started in October 2016 using an array of 12 antennas.

The MeerKAT is currently under construction in South African Karoo region. It is a precursor to the full SKA system but also operates as an independent instrument that will be conducting critical science for some years before being integrated into the SKA1. When completed it will be made of 64 dishes each of 13.5 m in diameter. The first seven dishes are complete and are known as KAT-7.

In addition to the SKA precursors, there are the SKA Pathfinders that will not be part of SKA but contribute to scientific and technical developments of direct use to the SKA (e.g., LOFAR).

The SKA science case is extensively discussed in the book "Advancing Astrophysics with the Square Kilometre Array" available at `https://www.skatelescope.org/books/`. The book comprises 135 chapters written by 1213 contributors. The science spans many diverse areas of astrophysics, with major advances expected in the following areas:

- Strong-field tests of gravity with pulsars and black holes.
- Cosmic dawn and the epoch of reionization.
- The transient radio sky.
- Cosmology and dark energy.
- The origin and evolution of cosmic magnetism.
- Galaxy evolution probed by neutral hydrogen.
- The cradle of life and astrobiology.
- Galaxy and cluster evolution probed in the radio continuum.

Studies of the star formation across cosmic time and of the galaxy-AGN co-evolution are among the top science priorities/drivers for continuum SKA1 surveys. A set of *reference surveys* have been identified (Prandoni & Seymour, 2015). Three of them are at $\simeq 1\,\mathrm{GHz}$, all with angular resolution of 0.5 arcsec, to avoid reaching the confusion limit:

- An ultra-deep survey (rms $0.05\,\mu\mathrm{Jy/beam}$) over an area of $1\,\mathrm{deg}^2$.

- A deep survey (rms $0.2\,\mu$Jy/beam) over an area of $10 - 30\,\mathrm{deg}^2$.
- A wide survey (rms $1\,\mu$Jy/beam) over an area of $1000\,\mathrm{deg}^2$.

According to the detailed predictions by Mancuso et al. (2015), the ultra-deep survey will detect, at $5\,\sigma$, high-z galaxies with SFRs two orders of magnitude lower compared to *Herschel* surveys, that were confusion limited. This means that SKA1 will reach SFRs of a few $M_\odot\,\mathrm{yr}^{-1}$ at $z \simeq 1$. The minimum detectable SFR increases with increasing redshift but is still of few $\times\, M_\odot\,\mathrm{yr}^{-1}$ at $z \simeq 10$, implying that the SKA1 ultra-deep survey can detect galaxies up to the highest redshifts, $z \simeq 10$.

The maximum redshift of detectable sources decreases to about 8 for the deep survey and to about 7 for the wide survey. Nevertheless, also these surveys will dig inside the re-ionization epoch. The highest redshift tails of the distributions at the detection limits of all these surveys comprise a substantial fraction of strongly lensed galaxies. Mancuso et al. (2015) predicted that the ultra-deep survey will detect about 1200 strongly lensed galaxies per square degree, at redshifts of up to 10. For about 30% of them the SKA1 will detect at least 2 images.

Two additional surveys, with a resolution of 0.1 arcsec, are foreseen at $\simeq 10\,\mathrm{GHz}$:

- An ultra-deep survey (rms $0.04\,\mu$Jy/beam) over an area of $0.0081\,\mathrm{deg}^2$.
- A deep survey (rms $0.3\,\mu$Jy/beam) over an area of $1\,\mathrm{deg}^2$.

Surveys at this higher frequency have two advantages compared to those at $\simeq 1\,\mathrm{GHz}$:

- They yield higher angular resolution, allowing us to resolve star-forming galaxies at substantial redshifts and to study the detailed astrophysics of star formation. They thus provide an extinction-free view for the morphologies of dusty star-bursting galaxies. These observations enable to distinguish between competing theories advocating either a star formation triggered by mergers or regulated by in-situ processes, or fuelled by large-scale flows of gas.
- At this frequency, emission of star-forming galaxies becomes dominated by free-free radiation. As discussed in section 4, at variance with synchrotron emission, the free-free is a measure of the instantaneous star formation rate, and allows the mapping of star-formation regions even in deeply dust-enshrouded regions.

In summary, the planned SKA1 continuum surveys will allow a great progress in the determination the star formation rate across cosmic times and in the understanding of the astrophysical processes going on within star forming galaxies. Also the SKA1 sensitivity and resolution will allow to detect nuclear activity down to very faint flux density levels, clarifying the radio properties of RQ AGNs. The large samples down to very faint flux densities provided by SKA1 surveys will enable a complete census of star-formation and AGN activity as a function of redshift, of galaxy mass and of galaxy morphology.

8 Conclusions

Radio astronomy has been playing a leading role in many fields of astronomical research. For decades, from the early 1950s to mid 1990s, identification of radio sources has remained the most effective method for finding high-z galaxies. Radio astronomical observations have led to Nobel prize discoveries (the CMB and its anisotropies,

the pulsars and their timing, allowing tests of general relativity in a strong gravitational field) as well as to other discoveries revolutionizing our understanding of the universe: the quasars and the ensuing understanding of black hole accretion as a powerful energy source, the cosmological evolution. In the 1950s they pushed the boundary of the observable universe far beyond the reach of optical telescopes of the time.

Radio source counts down to mJy flux density levels are dominated by radio AGNs. But a different population, star forming galaxies, is increasingly important at fainter and fainter flux densities, and becomes dominant below $\simeq 0.1$ mJy at 1.4 GHz. Hence, deep radio surveys are providing another tool to investigate the cosmic star formation history.

So far, radio surveys have played only a marginal role in this respect, but the SKA and, to some extent, its precursors will change this drastically, pushing the radio band at the forefront in terms of sensitivity to SFR in comparison to other bands.

The SKA2 is expected to detect, with a 1,000 h exposure, a galaxy with a SFR of $\sim 10\,M_\odot\,\mathrm{yr}^{-1}$ up to $z \sim 8$ (Murphy et al., 2015), thus providing a more complete view of the cosmic star formation than any other forthcoming instrument.

With 200 km baselines, observations at ~ 10 GHz will be able to achieve a maximum angular resolution $\lesssim 0.03$ arcsec, sampling 250 pc scales within disk galaxies at $z \sim 1$, providing an extinction-free view for the morphologies of dusty star-bursting galaxies that dominate the star formation activity between $1 \lesssim z \lesssim 3$.

While probing such fine physical scales requires sources that are extremely bright, the SKA should still have the sensitivity to easily resolve sub-$L_\star$ galaxies[6] at high redshifts (Murphy et al., 2015). SKA1-mid will easily resolve such sources at $z \lesssim 2$.

In the same redshift range, galaxies with $L_{\rm IR} \gtrsim 10^{12}\,L_\odot$ can be *mapped* by the SKA at ~ 10 GHz with a 0.1 arcsec resolution. Such resolution matches that of the JWST and enables a view of star formation activity even in the most dust-enshrouded regions.

These high-sensitivity, high angular resolution observations will shed light on the debated issue of the radio emission of RQ AGNs, distinguishing between the contribution from star formation and from AGN activity.

Acknowledgements. GDZ renews his appreciations for the kind invitation Third Cosmology School and the extraordinarily warm hospitality. Work supported in part by ASI/INAF agreement n. 2014-024-R.1 for the *Planck* LFI Activity of Phase E2 and by the ASI/Physics Department of the university of Roma–Tor Vergata agreement n. 2016-24-H.0 for study activities of the Italian cosmology community.

References

Alfvén, H., Herlofson, N., *Physical Review* **78**, 616 (1950)

Antonucci, R. R. J., Miller, J. S., *ApJ* **297**, 621 (1985)

Aversa, R., et al., *ApJ* **810**, 74 (2015)

Baade, W., Minkowski, R., *ApJ* **119**, 215 (1954)

[6] $L_\star$ galaxies at $1 \lesssim z \lesssim 3$ have total (8–1000 μm) infrared luminosities in the range $10^{11} \lesssim L_{\rm IR}/L_\odot \lesssim 10^{12}$

Baldi, R. D., Capetti, A., Giovannini, G., *A&A* **576**, A38 (2015)

Baloković, M., et al., *ApJ* **759**, 30 (2012)

Banday, A. J., Wolfendale, A. W., *MNRAS* **248**, 705 (1991)

Barcons, X., et al., in Journal of Physics Conference Series, *Journal of Physics Conference Series*, volume 610, 012008 (2015)

Barger, A. J., et al., *ApJ* **761**, 89 (2012)

Barger, A. J., et al., *ApJ* **835**, 95 (2017)

Barthel, P. D., *ApJ* **336**, 606 (1989)

Barvainis, R., et al., *ApJ* **618**, 108 (2005)

Begelman, M. C., Blandford, R. D., Rees, M. J., *Reviews of Modern Physics* **56**, 255 (1984)

Bell, E. F., *ApJ* **586**, 794 (2003)

Bolton, J. G., Stanley, G. J., Slee, O. B., *Nature* **164**, 101 (1949)

Bonato, M., et al., *MNRAS* **444**, 3446 (2014)

Bonato, M., et al., *MNRAS* **469**, 1912 (2017)

Bonchi, A., et al., *MNRAS* **429**, 1970 (2013)

Bonzini, M., et al., *ApJS* **203**, 15 (2012)

Bonzini, M., et al., *MNRAS* **436**, 3759 (2013)

Bonzini, M., et al., *MNRAS* **453**, 1079 (2015)

Burbidge, G. R., *ApJ* **129**, 849 (1959)

Cai, Z.-Y., et al., *ApJ* **768**, 21 (2013)

Cai, Z.-Y., et al., *ApJ* **785**, 65 (2014)

Calistro Rivera, G., et al., *MNRAS* **469**, 3468 (2017)

Chen, C.-T. J., et al., *ApJ* **773**, 3 (2013)

Chi, X., Wolfendale, A. W., *MNRAS* **245**, 101 (1990)

Cirasuolo, M., Celotti, A., Magliocchetti, M., Danese, L., *MNRAS* **346**, 447 (2003)

Cohen, M. H., et al., *ApJ* **170**, 207 (1971)

Combes, F., *Journal of Instrumentation* **10**, C09001 (2015)

Condon, J. J., *ApJ* **338**, 13 (1989)

Condon, J. J., *ARA&A* **30**, 575 (1992)

Condon, J. J., Mitchell, K. J., *AJ* **89**, 610 (1984)

Condon, J. J., et al., *ApJ* **768**, 37 (2013)

Danese, L., de Zotti, G., Franceschini, A., Toffolatti, L., *ApJL* **318**, L15 (1987)

de Zotti, G., Massardi, M., Negrello, M., Wall, J., *A&A Rev.* **18**, 1 (2010)

Delhaize, J., et al., *A&A* **602**, A4 (2017)

Delvecchio, I., et al., *A&A* **602**, A3 (2017)

Dicke, R. H., Peebles, P. J. E., Roll, P. G., Wilkinson, D. T., *ApJ* **142**, 414 (1965)

Donley, J. L., et al., *ApJ* **748**, 142 (2012)

Fanaroff, B. L., Riley, J. M., *MNRAS* **167**, 31P (1974)

Gardner, J. P., in Space Telescopes and Instrumentation 2012: Optical, Infrared, and Millimeter Wave, *Proc. SPIE*, volume 8442, 844228 (2012)

Ginzburg, V. L., Syrovatskii, S. I., *ARA&A* **3**, 297 (1965)

Giroletti, M., Panessa, F., *ApJL* **706**, L260 (2009)

Gold, B., et al., *ApJS* **192**, 15 (2011)

Grainge, K., et al., *Astronomy Reports* **61**, 288 (2017)

Greenhouse, M., *IAU General Assembly* **22**, 2219646 (2015)

Guidetti, D., et al., *MNRAS* **432**, 2798 (2013)

Hazard, C., Mackey, M. B., Shimmins, A. J., *Nature* **197**, 1037 (1963)

Helou, G., Soifer, B. T., Rowan-Robinson, M., *ApJL* **298**, L7 (1985)

Herrera Ruiz, N., Middelberg, E., Norris, R. P., Maini, A., *A&A* **589**, L2 (2016)

Hewish, A., et al., *Nature* **217**, 709 (1968)

Hoyle, F., *Nature* **209**, 751 (1966)

Hoyle, F., Burbidge, G. R., *ApJ* **144**, 534 (1966)

Hoyle, F., Fowler, W. A., *Nature* **197**, 533 (1963)

Hulse, R. A., Taylor, J. H., *ApJL* **195**, L51 (1975)

Ivezić, Ž., et al., *AJ* **124**, 2364 (2002)

Ivezić, Z., et al., in G. T. Richards, P. B. Hall (eds.) AGN Physics with the Sloan Digital Sky Survey, *Astronomical Society of the Pacific Conference Series*, volume 311, 347 (2004)

Ivison, R. J., et al., *A&A* **518**, L31 (2010)

Jackson, N., et al., *MNRAS* **454**, 287 (2015)

Kellermann, K. I., et al., *AJ* **98**, 1195 (1989)

Kimball, A. E., et al., *ApJL* **739**, L29 (2011)

Klein, U., Wielebinski, R., Thuan, T. X., *A&A* **141**, 241 (1984)

Kron, R. G., Koo, D. C., Windhorst, R. A., *A&A* **146**, 38 (1985)

Lacki, B. C., Thompson, T. A., *ApJ* **717**, 196 (2010)

Lacki, B. C., Thompson, T. A., Quataert, E., *ApJ* **717**, 1 (2010)

Lacy, M., et al., *ApJL* **551**, L17 (2001)

Lacy, M., et al., *ApJS* **154**, 166 (2004)

Leitherer, C., et al., *ApJS* **123**, 3 (1999)

Liske, J., Padovani, P., Kissler-Patig, M., in Ground-based and Airborne Telescopes IV, *Proc. SPIE*, volume 8444, 84441I (2012)

LSST Science Collaboration, et al., *arXiv e-prints* (2017)

Lynden-Bell, D., *Nature* **223**, 690 (1969)

Magnelli, B., et al., *A&A* **573**, A45 (2015)

Mancuso, C., et al., *ApJ* **810**, 72 (2015)

Massardi, M., et al., *MNRAS* **404**, 532 (2010)

Massardi, M., et al., *MNRAS* **412**, 318 (2011)

Mauch, T., Sadler, E. M., *MNRAS* **375**, 931 (2007)

Mills, B. Y., Slee, O. B., *Australian Journal of Physics* **10** (1957)

Mills, B. Y., Slee, O. B., Hill, E. R., *Australian Journal of Physics* **11**, 360 (1958)

Minkowski, R., *ApJ* **132**, 908 (1960)

Moffet, A. T., Gubbay, J., Robertson, D. S., Legg, A. J., in D. S. Evans, D. Wills, B. J. Wills (eds.) External Galaxies and Quasi-Stellar Objects, *IAU Symposium*, volume 44, 228 (1972)

Molnár, D. C., et al., *MNRAS* **475**, 827 (2018)

Murphy, E., et al., *Advancing Astrophysics with the Square Kilometre Array (AASKA14)* 85 (2015)

Murphy, E. J., et al., *ApJ* **737**, 67 (2011)

Murphy, E. J., et al., *ApJ* **761**, 97 (2012)

Nakagawa, T., et al., *Publication of Korean Astronomical Society* **32**, 331 (2017)

Norris, R. P., et al., *PASA* **30**, e020 (2013)

Orienti, M., *Astronomische Nachrichten* **337**, 9 (2016)

Orr, M. J. L., Browne, I. W. A., *MNRAS* **200**, 1067 (1982)

Padovani, P., *A&A Rev.* **24**, 13 (2016)

Padovani, P., et al., *MNRAS* **452**, 1263 (2015)

Padovani, P., et al., *A&A Rev.* **25**, 2 (2017)

Pappalardo, C., et al., *A&A* **573**, A129 (2015)

Penzias, A. A., Wilson, R. W., *ApJ* **142**, 419 (1965)

Planck Collaboration, et al., *A&A* **594**, A26 (2016)

Prandoni, I., Seymour, N., *Advancing Astrophysics with the Square Kilometre Array (AASKA14)* 67 (2015)

Price, R., Duric, N., *ApJ* **401**, 81 (1992)

Rees, M. J., *Nature* **211**, 468 (1966)

Ryle, M., *The Observatory* **75**, 137 (1955)

Ryle, M., *ARA&A* **6**, 249 (1968)

Ryle, M., Clarke, R. W., *MNRAS* **122**, 349 (1961)

Ryle, M., Scheuer, P. A. G., *Proceedings of the Royal Society of London Series A* **230**, 448 (1955)

Ryle, M., Smith, F. G., Elsmore, B., *MNRAS* **110**, 508 (1950)

Sadler, E. M., et al., *MNRAS* **329**, 227 (2002)

Salpeter, E. E., *ApJ* **140**, 796 (1964)

Sandage, A., *ApJ* **141**, 1560 (1965)

Scheuer, P. A. G., *Proceedings of the Cambridge Philosophical Society* **53**, 764 (1957)

Scheuer, P. A. G., in J. A. Zensus, T. J. Pearson (eds.) Superluminal Radio Sources, 104–113 (1987)

Scheuer, P. A. G., Readhead, A. C. S., *Nature* **277**, 182 (1979)

Schleicher, D. R. G., Beck, R., *A&A* **556**, A142 (2013)

Schmidt, M., *Nature* **197**, 1040 (1963)

Schmidt, M., *ApJ* **141**, 1295 (1965)

Shakeshaft, J. R., et al., *MmRAS* **67**, 106 (1955)

Sheth, R. K., Tormen, G., *MNRAS* **308**, 119 (1999)

Shklovskii, I. S., *AZh* **29**, 418 (1952)

Smith, F. G., *MNRAS* **112**, 497 (1952)
Smolčić, V., et al., *A&A* **602**, A2 (2017)
Smoot, G. F., et al., *ApJL* **396**, L1 (1992)
Spergel, D., et al., *arXiv e-prints* (2015)
Steidel, C. C., et al., *ApJL* **462**, L17 (1996)
Stern, D., *PASP* **112**, 1411 (2000)
Stern, D., et al., *AJ* **119**, 1526 (2000)
Urry, C. M., Padovani, P., *PASP* **107**, 803 (1995)
White, S. V., Jarvis, M. J., Häußler, B., Maddox, N., *MNRAS* **448**, 2665 (2015)
Whitney, A. R., et al., *Science* **173**, 225 (1971)
Wilkinson, P. N., et al., *New A Rev.* **48**, 1551 (2004)
Windhorst, R. A., van Heerde, G. M., Katgert, P., *A&AS* **58**, 1 (1984)
Windhorst, R. A., et al., *ApJ* **289**, 494 (1985)
Woltjer, L., *ApJ* **146**, 597 (1966)
York, D. G., et al., *AJ* **120**, 1579 (2000)
Yun, M. S., Reddy, N. A., Condon, J. J., *ApJ* **554**, 803 (2001)
Zakamska, N. L., et al., *MNRAS* **455**, 4191 (2016)
Zel'dovich, Y. B., *Soviet Physics Doklady* **9**, 195 (1964)